

Supplementary Materials

High-precision electrohydrodynamic printing of EGaIn-AgNPs biphasic conductive ink for conformal and lightweight bioelectrodes

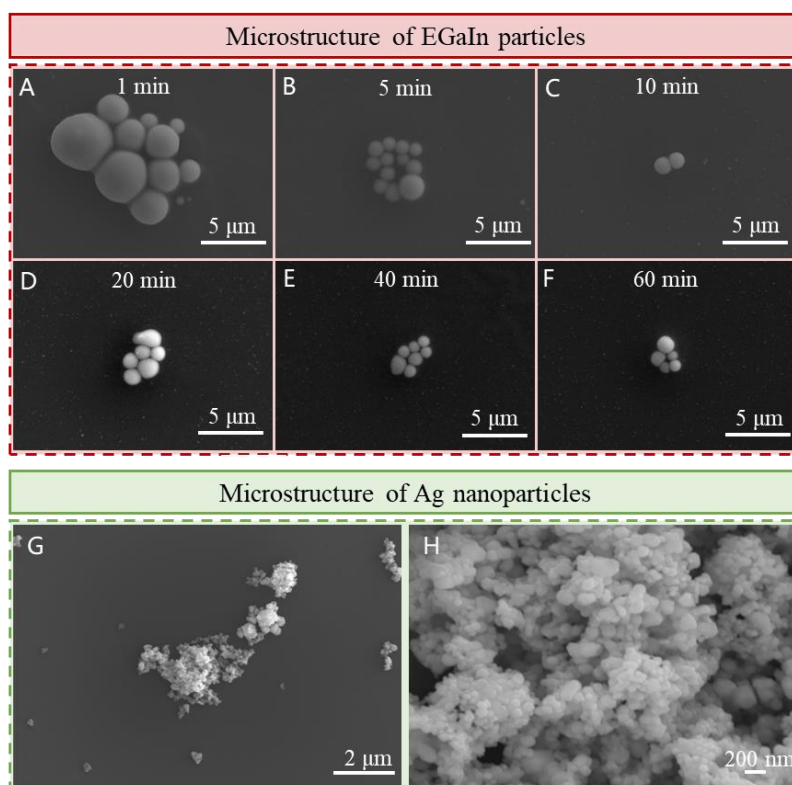
Jingxuan Ma¹, Jiayun Feng^{1,2}, Zicheng Sa¹, Fanzhou Meng¹, Zhao Feng¹, Qing Sun^{1,2,3}, Yuxin Sun¹, Jiayue Wen², Shang Wang^{1,2}, Yanhong Tian^{1,2}

¹State Key Laboratory of Precision Welding and Joining of Materials and Structures, Harbin Institute of Technology, Harbin 150001, Heilongjiang, China.

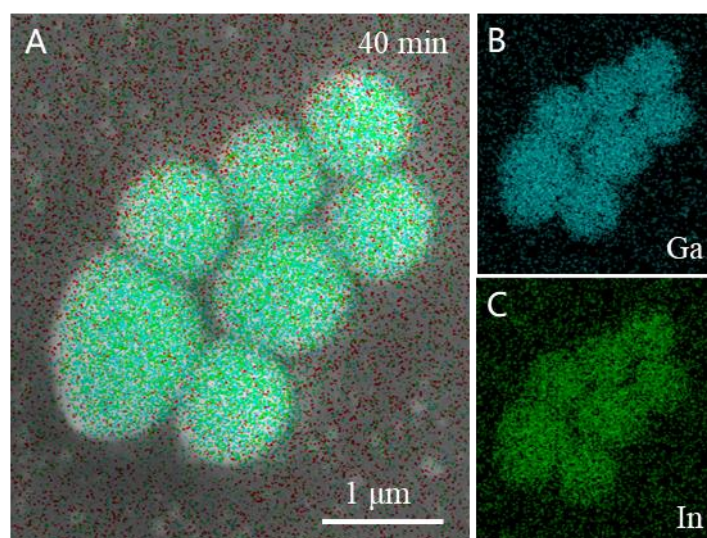
²Zhengzhou Research Institute, Harbin Institute of Technology, Zhengzhou 450041, Henan, China.

³Catalonia Institute for Energy Research - IREC, Barcelona 08930, Spain.

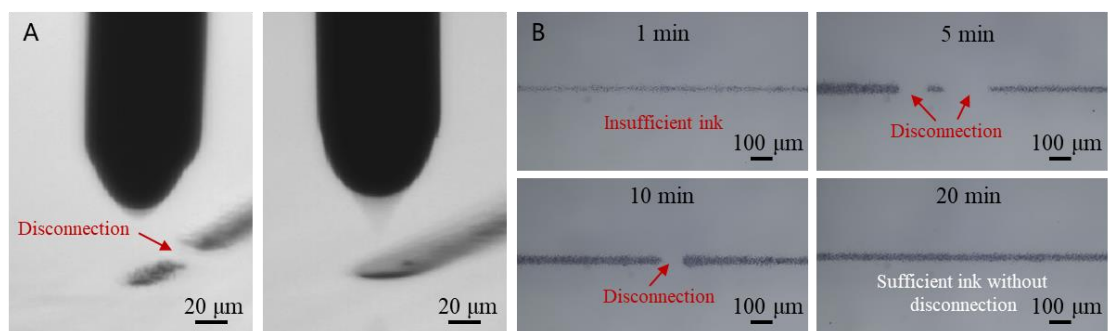
Correspondence to: Dr. Jiayun Feng, Prof. Yanhong Tian, State Key Laboratory of Precision Welding and Joining of Materials and Structures, Harbin Institute of Technology, Harbin 150001, Heilongjiang, China. E-mail: fengjy@hit.edu.cn; tianyh@hit.edu.cn



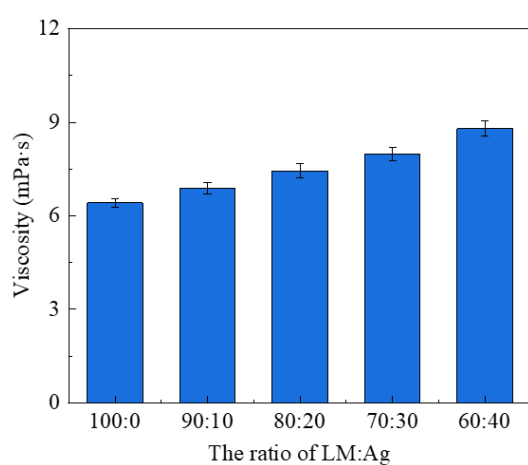
Supplementary Figure 1. Microstructure of EGaIn particles and Ag nanoparticles. EGaIn particles under ultrasonic time of (A) 1 min, (B) 5 min, (C) 10 min, (D) 20 min, (E) 40 min and (F) 60 min. SEM image of AgNPs under (G) low magnification and (H) high magnification.



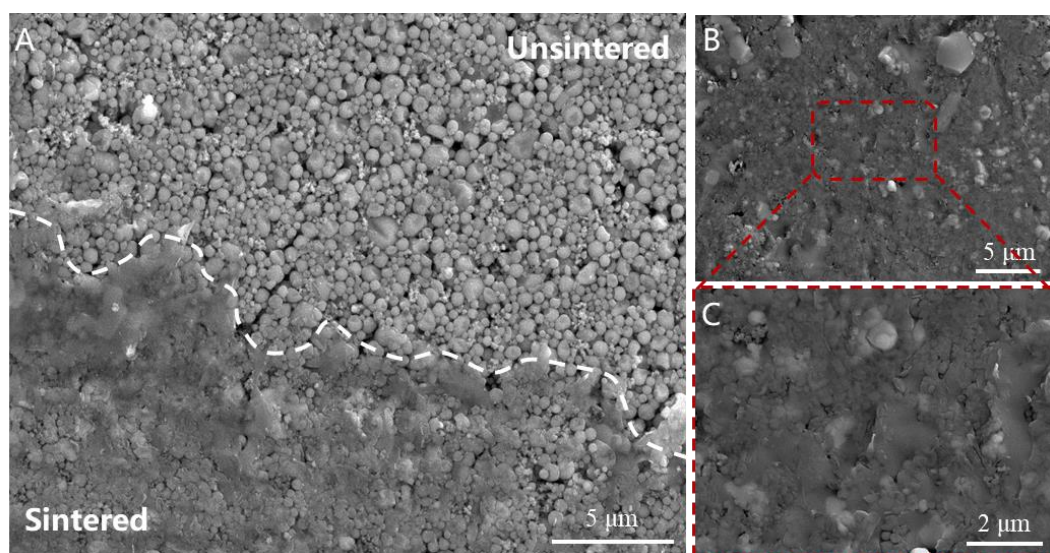
Supplementary Figure 2. Surface scanning analysis of EGaIn particles (40 min ultrasonic treatment). (A) Merged image. EDS mapping results of (B) Ga and (C) In.



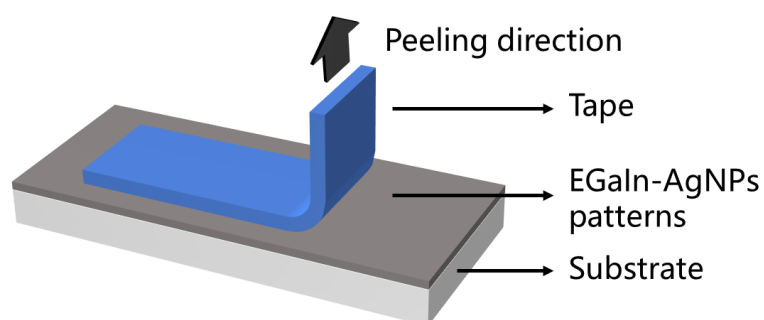
Supplementary Figure 3. Effects of different ultrasonic treatment time on EHD printing quality. (A) Discontinuous printing and normal printing mode. (B) Optical microscope photos of printed lines under different ultrasonic treatment times.



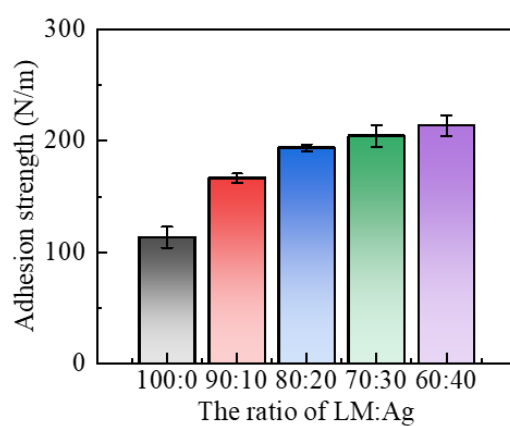
Supplementary Figure 4. The viscosity at different ratios of LM and Ag.



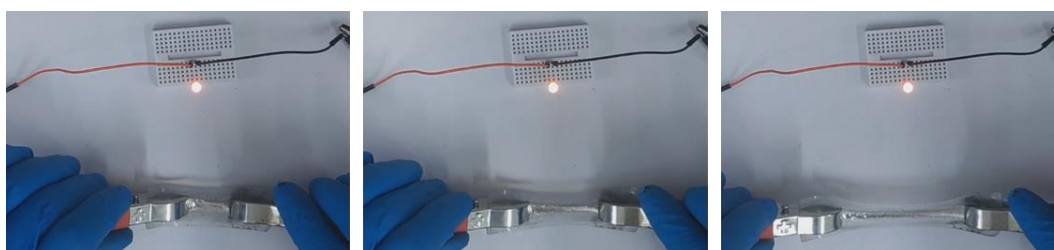
Supplementary Figure 5. Mechanical sintering of EGaIn-AgNPs ink. (A) Boundary between sintered area and unsintered area. (B) Microstructure of sintering area. (C) Enlarged view.



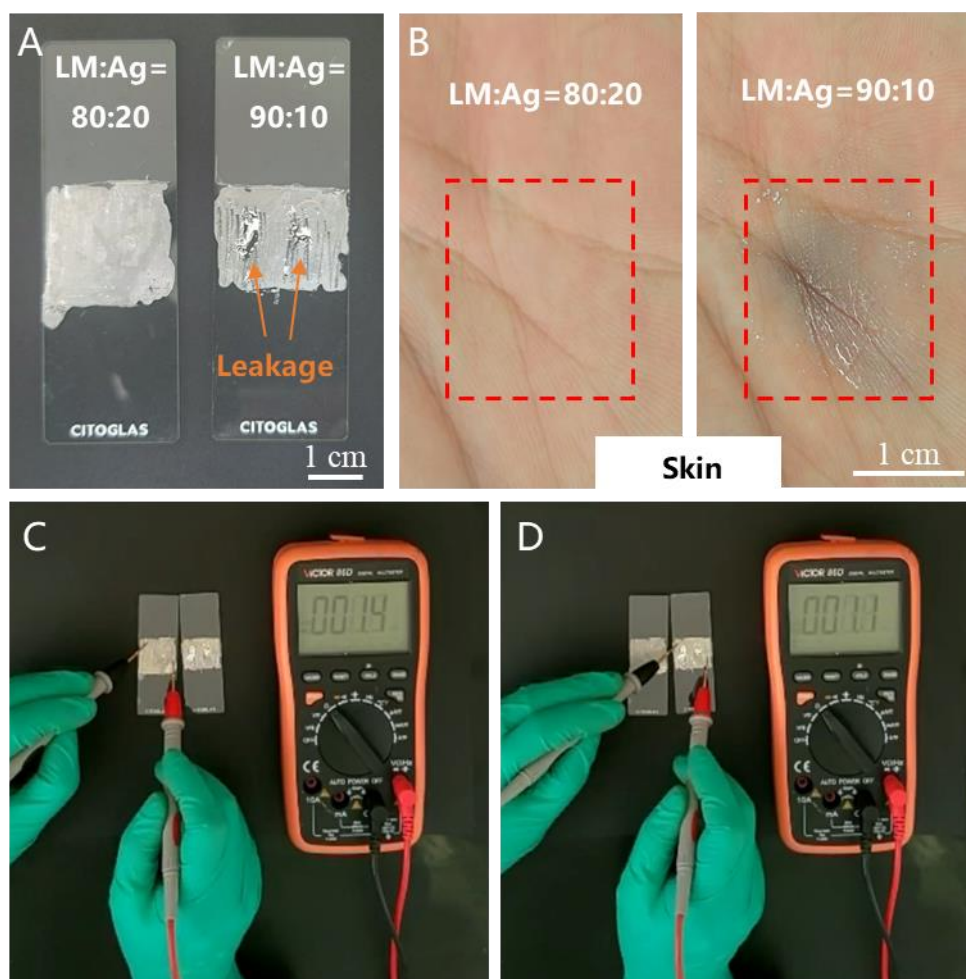
Supplementary Figure 6. Schematic illustration of adhesion strength test.



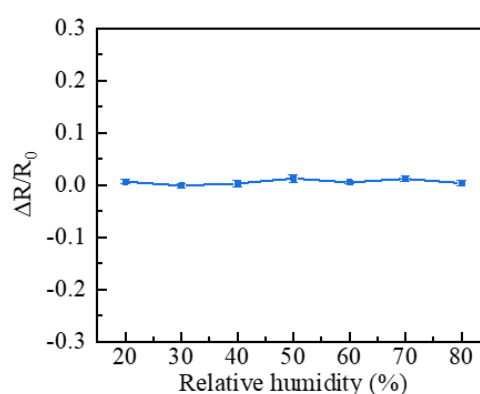
Supplementary Figure 7. Adhesion strength of EGaIn-AgNPs inks with different ratios.



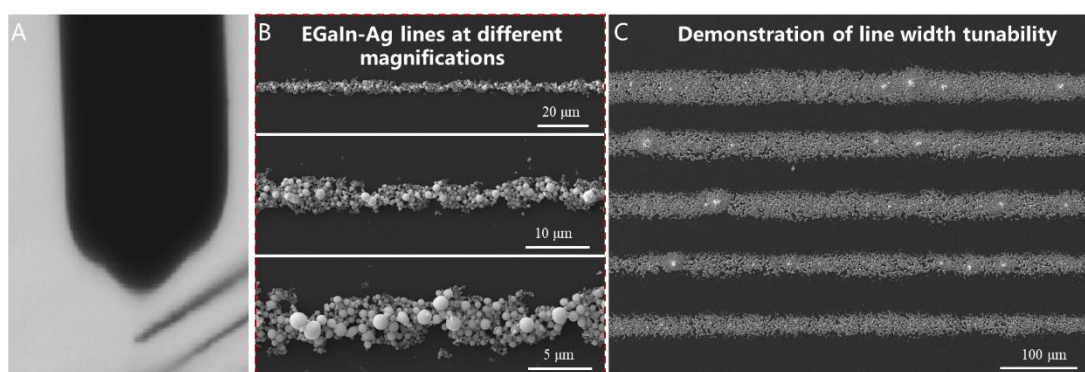
Supplementary Figure 8. Demonstration of stretchability of EGaIn-AgNPs electrodes.



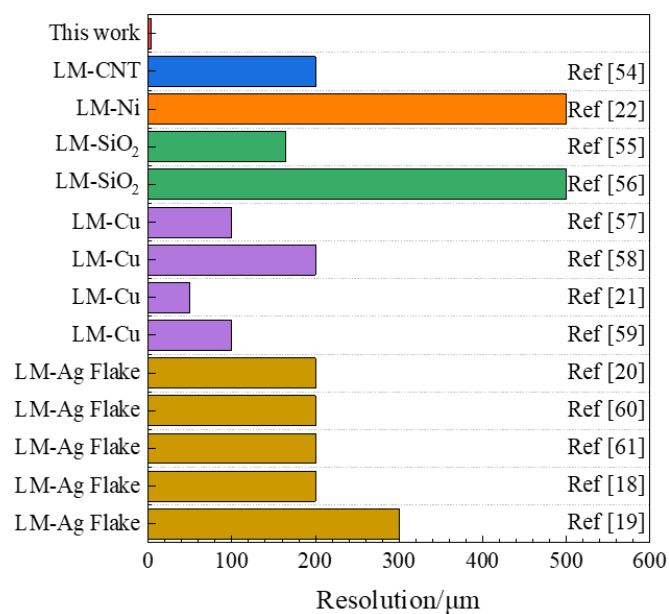
Supplementary Figure 9. Leakage test of EGaIn-AgNPs conductive ink. (A) Comparison of leakage between LM=Ag=80:20 and LM:Ag=90:10 inks after mechanical sintering. (B) Photographs of human skin after applying electrodes made of two types of inks. Electrical conductivity after mechanical sintering for LM:Ag ratios of (C) 80:20 and (D) 90:10.



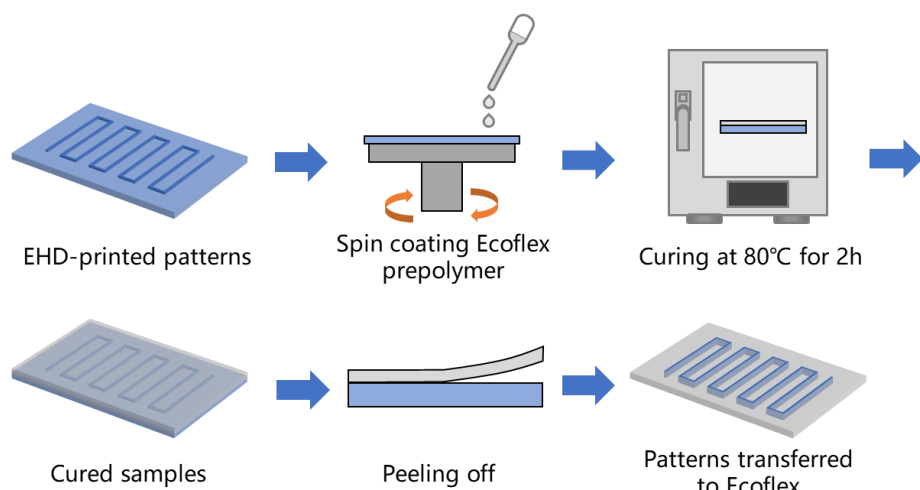
Supplementary Figure 10. Humidity stability test of EGaIn-AgNPs structure.



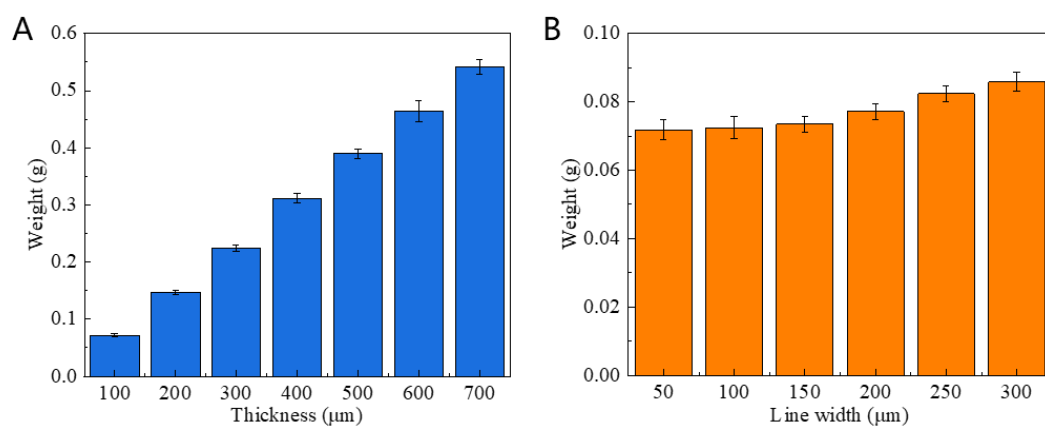
Supplementary Figure 11. EHD printing process of EGaIn-AgNPs ink. (A) Optical image of the Taylor cone during EHD printing. (B) EHD-printed EGaIn-Ag lines. (C) Demonstration of line width tunability.



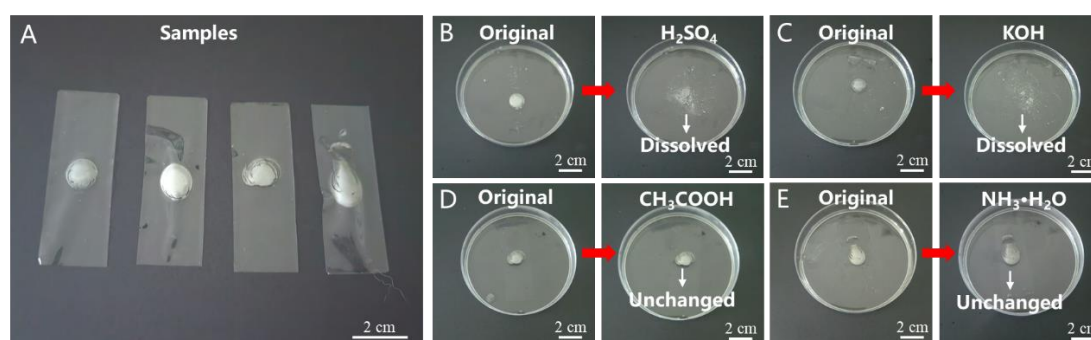
Supplementary Figure 12. Comparison of patterning resolution of LM-based biphasic conductive inks with reported literature.



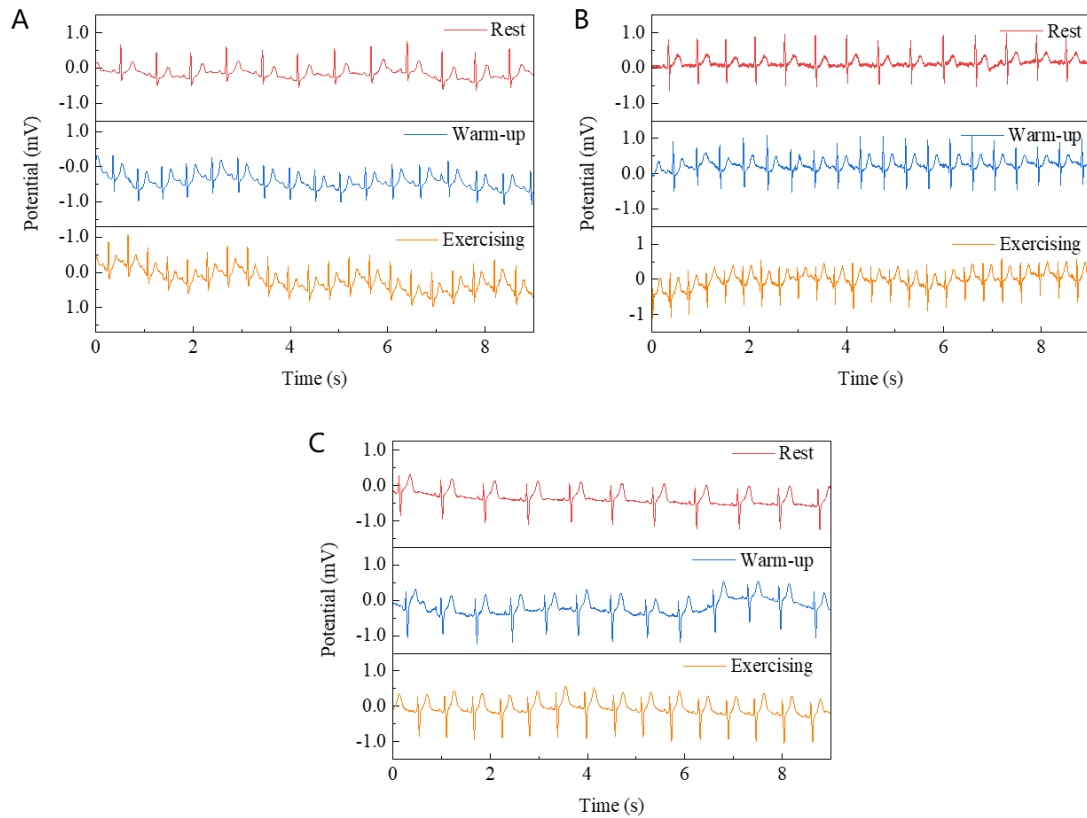
Supplementary Figure 13. Schematic diagram of the transfer process.



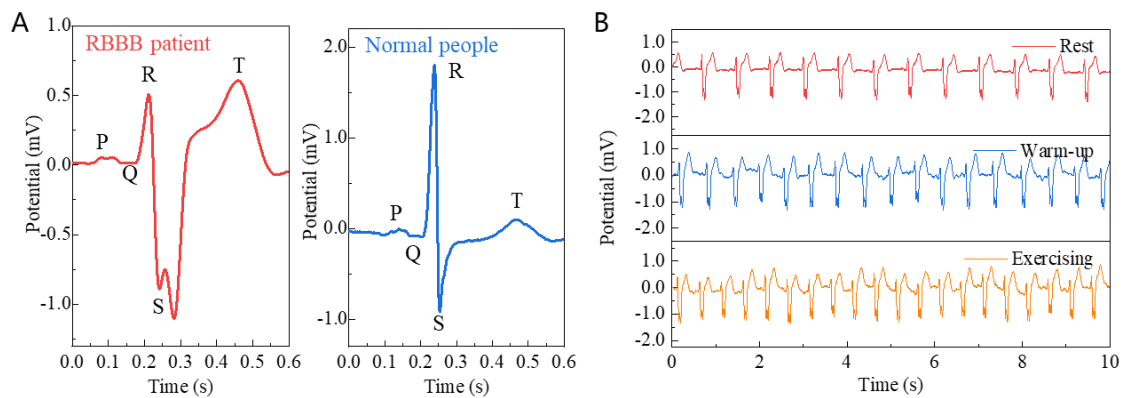
Supplementary Figure 14. Electrode weight under different thickness and printing line width. (A) Thickness. (B) Line width.



Supplementary Figure 15. Corrosion resistance test. (A) Prepared samples. (B) Strong acid (H_2SO_4). (C) Strong base (KOH). (D) Weak acid (CH_3COOH). (E) Weak base ($\text{NH}_3\cdot\text{H}_2\text{O}$).



Supplementary Figure 16. ECG test results of three volunteers based on EGaln-AgNPs electrodes. (A) Young female volunteer who exercises regularly. (B) Male volunteer who exercises infrequently. (C) Male volunteer who exercises regularly.



Supplementary Figure 17. Abnormal ECG (right bundle branch block) test results based on EGaln-AgNPs electrodes. (A) Comparison of ECG between RBBB patients and normal people. (B) ECG monitoring signals during rest, warm-up and exercise.

Supplementary Table 1. Comparison of patterning resolution of LM-based biphasic conductive inks with reported literature

Ink component	Resolution/ μm	Patterning method	Reference
LM-AgNP	3.15	EHD printing	This work
LM-CNT	200	Stencil printing	54
LM-Ni	500	Stencil printing	22
LM-SiO ₂	165	Direct ink printing	55
LM-SiO ₂	500	3D printing	56
LM-Cu	100	Laser-printing-assisted printing	57
LM-Cu	200	Screen printing	58
LM-Cu	50	Thermal printing	21
LM-Cu	100	Laser-printing-assisted printing	59
LM-Ag Flake	200	Inkjet printing	20
LM-Ag Flake	200	Inkjet printing	60
LM-Ag Flake	200	Inkjet printing	61
LM-Ag Flake	200	Inkjet printing	18
LM-Ag Flake	300	Inkjet printing	19

REFERENCES

18. Tavakoli, M.; Malakooti, M. H.; Paisana, H.; et al. Egain-assisted room-temperature sintering of silver nanoparticles for stretchable, inkjet-printed, thin-film electronics. *Adv. Mater.* **2018**, *30* (29), 1801852. <https://doi.org/10.1002/adma.201801852>.
19. Reis Carneiro, M.; Majidi, C.; Tavakoli, M. Multi-electrode printed bioelectronic patches for long-term electrophysiological monitoring. *Adv. Funct. Mater.* **2022**, *32* (43), 2205956. <https://doi.org/10.1002/adfm.202205956>.
20. Lopes, P. A.; Santos, B. C.; de Almeida, A. T.; et al. Reversible polymer-gel transition for ultra-stretchable chip-integrated circuits through self-soldering and self-coating and self-healing. *Nat. Commun.* **2021**, *12* (1), 4666. 10.1038/s41467-021-25008-5.
21. Guo, R.; Li, T.; Wu, Z.; et al. Thermal transfer-enabled rapid printing of liquid metal circuits on multiple substrates. *ACS Appl. Mater. Interfaces.* **2022**, *14* (32), 37028-37038. 10.1021/acsami.2c08743.
22. Wu, Y.-h.; Deng, Z.-f.; Peng, Z.-f.; et al. A novel strategy for preparing stretchable and reliable biphasic liquid metal. *Adv. Funct. Mater.* **2019**, *29* (36), 1903840. <https://doi.org/10.1002/adfm.201903840>.
54. Lee, G.-H.; Woo, H.; Yoon, C.; et al. A personalized electronic tattoo for healthcare realized by on-the-spot assembly of an intrinsically conductive and durable liquid-metal composite. *Adv. Mater.* **2022**, *34* (32), 2204159. <https://doi.org/10.1002/adma.202204159>.
55. Chen, W.; Tang, Q.; Zhong, W.; et al. Directly printable and adhesive liquid metal ink for wearable devices. *Adv. Funct. Mater.* **2025**, *35* (1), 2411647. <https://doi.org/10.1002/adfm.202411647>.
56. Qiu, Y.; Zou, Z.; Zou, Z.; et al. Deep-learning-assisted printed liquid metal sensory system for wearable applications and boxing training. *npj Flex. Electron.* **2023**, *7* (1), 37. 10.1038/s41528-023-00272-1.
57. Zhao, R.; Guo, R.; Xu, X.; et al. A fast and cost-effective transfer printing of liquid metal inks for three-dimensional wiring in flexible electronics. *ACS Appl. Mater. Interfaces.* **2020**, *12* (32), 36723-36730. 10.1021/acsami.0c08931.
58. Kim, M. S.; Kim, S.; Choi, J.; et al. Stretchable printed circuit board based on leak-free liquid metal interconnection and local strain control. *ACS Appl. Mater. Interfaces.*

2022, *14* (1), 1826-1837. 10.1021/acsami.1c16177.

59. Guo, R.; Cui, B.; Zhao, X.; et al. Cu–egain enabled stretchable e-skin for interactive electronics and ct assistant localization. *Mater. Horiz.* **2020**, *7* (7), 1845-1853. 10.1039/C9MH02066G.

60. Lopes, P. A.; Fernandes, D. F.; Silva, A. F.; et al. Bi-phasic ag–in–ga-embedded elastomer inks for digitally printed, ultra-stretchable, multi-layer electronics. *ACS Appl. Mater. Interfaces.* **2021**, *13* (12), 14552-14561. 10.1021/acsami.0c22206.

61. Reis Carneiro, M.; de Almeida, A. T.; Tavakoli, M.; et al. Recyclable thin-film soft electronics for smart packaging and e-skins. *Adv. Sci.* **2023**, *10* (26), 2301673. <https://doi.org/10.1002/advs.202301673>.